Chapter 4. Space Charge and Beam Stability

D. Carey, V. Dunikov, K.Y. Ng, C. Prior, B. Zotter

4.1 Space Charge and Image Effects

4.1.1 Incoherent Betatron Tune Shifts

The *betatron tunes* ν_z , $z = x$ or y, of transverse oscillations of charged particles in the beam moving with axial velocity $v = \beta c$, c being the velocity of light, are mainly determined by the applied focusing forces due to quadrupoles. With finite beam current the tunes are shifted, both by direct space charge and by "image" forces due to induced voltages in the surrounding structure impedances. At relativistic beam energies, the space charge forces are strongly reduced by a factor $\gamma^{-2} = 1 - \beta^2$ (with γ being the particle energy E in units of its rest energy) due to partial compensation of electric and magnetic forces. However, in the Proton Driver at 400 MeV injection energy, γ = 1.426 and the space charge term is then largely dominant.

The vertical *incoherent tune shift* of a transversely uniform beam of elliptic cross section, with half width a_x and half height a_y, consisting of N protons with classical radius r_p, with bunching factor B_f, the ratio of average to peak current, circulating in a vacuum chamber of half height b, inside a magnet gap of half-height g extending over a fraction κ of the machine circumference, is given by [1]

$$\Delta\nu_z = -\frac{N r_p \langle\beta_z\rangle}{\pi\beta^2\gamma}\left[\frac{\gamma^{-2}-\chi_e}{B_f\, a_z(a_x+a_y)} + \left(\beta^2 + \frac{\gamma^{-2}-\chi_e}{B_f}\right)\frac{\epsilon_{1z}}{b^2} + \kappa\beta^2\frac{\epsilon_{2z}}{g^2}\right] , \qquad (4.1)$$

where $\langle\beta_z\rangle \approx R/\nu_z$ is the average value of the betatron function, R the average radius of the ring, χ_e the fractional *neutralization* which reduces the electric but not the magnetic force, thus perturbing their compensation. The *Laslett coefficients* $\varepsilon_{1,2z}$ describe the strength of image forces for a particular geometry. A number are shown in Table 4.1; here we take parallel-plate values.

Except for large neutralizations at high energies (when $\chi_e > \gamma^{-2}$), the space charge tune shift is always negative. This is the first term in Eq. (4.1) and is also known as *tune depression*. Since the vertical Laslett coefficients are positive, these image terms add to the space charge tune shift, while they reduce it in the horizontal direction.

The reduction of bunch length and transverse dimensions during acceleration was obtained by computer simulation [2]. The evolution of tune shifts during an acceleration cycle has been calculated from Eq. (4.1) with the program TUNES written in MATHEMATICA [3]. The results for $\chi_e = 0$ are shown in Fig. 4.1 and Table 4.2. For small neutralizations the incoherent tune shifts are actually reduced. The parameters used

for Fig. 4.1 and Table 4.1 were ring circumference C = 711.2 m, particle kinetic energy E_{kin} = 400 MeV, betatron tune $\nu_z = 11.4$, average betatron function $\langle\beta_z\rangle$ = 9.92 m, normalized 95% emittance $\varepsilon = 60 \times 10^{-6}$ πm, full energy spread $\Delta E/E = 7 \times 10^{-4}$, average dispersion $\langle D_x\rangle$ = 1.27 m, average half beam width $a_{x,y}$ = 25.0 and 24.2 mm, beam pipe radius b = 63 mm, magnet half gap g = 64 mm covering κ = 0.5 of the ring, zero neutralization, and bunching factor at injection $B_f = 0.5$.

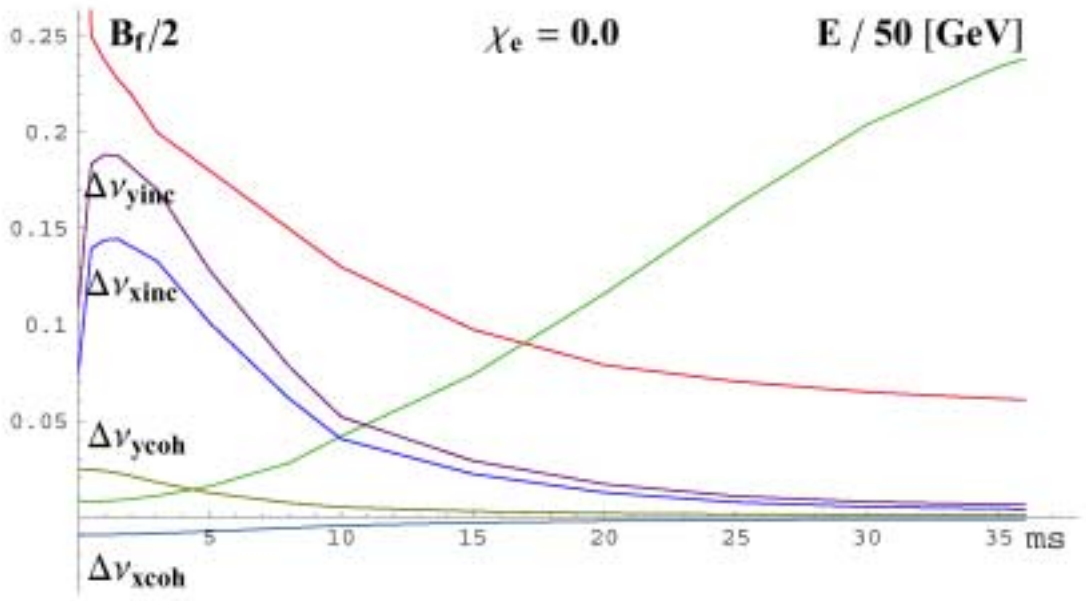

Figure 4.1. Bunching factor, energy and tune shifts during one acceleration cycle

The largest incoherent tune shifts occur 1–2 ms after injection, when the beam energy is still low, but the bunch length had decreased strongly when the protons were captured in the rf field.

Table 4.1. Laslett Coefficients at center of various cross sections

Geometry	ϵ_{1v}	ϵ_{1h}	ξ_{1v}	ξ_{1h}	$\xi_{1v}-\epsilon_{1v}$	$\xi_{1h}-\epsilon_{1h}$
parallel plate	0.205	−0.205	0.615	0.0	0.410	0.205
rectangular 5:9	0.188	−0.188	0.600	0.035	0.411	0.223
elliptic 5:9	0.162	−0.162	0.592	0.107	0.430	0.269
circular	0.000	−0.000	0.500	0.500	0.500	0.500

It is usually considered prudent to keep all tunes away from low-order resonances, in particular from integer multiples of the revolution frequency. Therefore conservative tune shift limits of 0.25 are often assumed, and it is satisfying that the estimates given above do not exceed this limit. However, if the transverse distribution of particles is not uniform but peaked, the space charge tune shift is up to 300% higher, with bi-Gaussian

distribution, for example. Values obtained by computer simulation were slightly above 0.25 in the vertical, and just below it in the horizontal direction.

However, since the dominant space charge force is generated inside a particle beam itself, it actually does not deflect the beam and thus cannot drive it into *dipole resonances* [4]. This can be seen from the equation for betatron oscillations of a particle with offset y from the center of the vacuum chamber, in the presence of (normalized) image and space-charge forces F_{im} and F_{sc}, which are

$$\frac{d^2y}{dt^2} + (\nu_y\omega_0)^2 y = F_{im}y + F_{sc}(y - \bar{y}) \tag{4.2}$$

where $\bar{y}$ is the offset of the beam center. Averaging over all particles yields

$$\frac{d^2\bar{y}}{dt^2} + (\nu_y\omega_0)^2 \bar{y} = F_{im}\bar{y} \tag{4.3}$$

i.e., the driving term for the space charge effect vanishes, while the image term causes a shift of the *coherent tune* to $\nu_{\rm coh}^2 = \nu_{y0}^2 - F_{im}/\omega_0^2$.

Table 4.2. (Negative) Space charge and Image Tune Shifts

t [ms]	$\Delta\nu_{xsc}$	$\Delta\nu_{xim}$	$\Delta\nu_{xinc}$	$\Delta\nu_{xcoh}$	$\Delta\nu_{ysc}$	$\Delta\nu_{yim}$	$\Delta\nu_{yinc}$	$\Delta\nu_{ycoh}$
0	0.089	−0.0213	0.0678	0.0156	0.092	0.0213	0.114	0.0310
1	0.163	−0.0256	0.1376	0.0154	0.169	0.0256	0.194	0.0299
2	0.159	−0.0241	0.1347	0.0148	0.164	0.0241	0.188	0.0271
5	0.113	−0.0167	0.0963	0.0120	0.116	0.0167	0.133	0.0170
10	0.045	−0.0078	0.0381	0.0069	0.047	0.0078	0.055	0.0076
20	0.015	−0.0032	0.0116	0.0031	0.015	0.0032	0.018	0.0031
30	0.007	−0.0019	0.0047	0.0019	0.007	0.0019	0.009	0.0019
38	0.005	−0.0016	0.0037	0.0016	0.005	0.0016	0.007	0.0016

4.1.2 Coherent Betatron Tune Shifts

The coherent tune shifts are given by the same equations as the incoherent ones, but without the space charge term and with the Laslett coefficients $\varepsilon_{1,2z}$ replaced by $\xi_{1,2z}$. However, for the usual case of a chamber wall thick enough that ac magnetic fields do not penetrate, the term $\beta^2\varepsilon_{1z}/b^2$ remains unchanged [5]:

$$\Delta\nu_z = -\frac{Nr_p\langle\beta_z\rangle}{\pi\beta^2\gamma}\left[\beta^2\frac{\epsilon_{1z}}{b^2} + \frac{\gamma^{-2} - \chi_\epsilon}{B_f}\frac{\xi_{1z}}{b^2} + \kappa\beta^2\frac{\xi_{2z}}{g^2}\right] . \tag{4.4}$$

In a flat chamber, $\xi_{1y} = \xi_{2y} = \pi^2/16$, while both ξ_{1x} = ξ_{2x} = 0. For a 5:9 rectangular chamber, ξ_{1y} = 0.60 and ξ_{1x} = 0.035, with similar values for an elliptic one.

The direct space charge force does not affect dipole oscillations, but it does change the external focusing forces. In one dimension, the evolution of the beam size a_z ($z = x$ or y) is described by the *envelope equation*

$$\frac{d^2 a_z}{ds^2} + K_z(s) a_z - \frac{\epsilon_z}{a_z^3} = \frac{4\lambda r_p}{\beta^2\gamma^3(a_x + a_y)} \qquad (4.5)$$

where $K_z(s)$ is the external focusing strength, ε_z the unnormalized transverse emittance, λ the number of particles per unit length.

The space charge force leads to a *modulation of the beam envelope*, which reduces the tune shift of the lowest *quadrupole mode* to $\frac{3}{4}\,\nu_{\rm sc}$. For the 2-dimensional case, there are 2 modes of quadrupole oscillations: the *antisymmetric mode* has its tune shift also reduced to $\frac{3}{4}\,\nu_{\rm sc}$, and the *symmetric mode* even to $\frac{1}{2}\,\nu_{\rm sc}$. Hence these modes are not excited when only the *incoherent tune* crosses (half-) integer resonances. Nevertheless, one has to allow for a variation of tunes during acceleration due to incomplete tracking of quadrupole and dipole strengths, and therefore one needs a certain safety margin to these resonances. In Phase I of the Proton Driver, tune shifts do not exceed 0.25, which can be safely accommodated with a properly chosen working point.

Higher order oscillations—sextupole, octupole, etc—have larger space charge tune shifts, but have not been observed in simulation nor in actual machines. They are suppressed by *Landau damping* due to the nonlinearity of space charge forces.

4.1.3 Longitudinal space charge effects

The *coherent synchrotron frequency* of a bunch is nearly constant with current since the coherent and incoherent longitudinal tune shifts cancel, $\Delta\nu_{\rm s,coh} = -\Delta\nu_{\rm s,inc}$. At low energies the incoherent frequency shift of Gaussian beam can be written [6]

$$\Delta\nu_{s,inc} = -\frac{3Nr_p\eta R^2}{2\beta^2\gamma^3\nu_{s0}}\frac{g_f}{L_b^3}\ , \qquad (4.6)$$

where L_b is the full bunch length, and g_f is commonly known as the *g-factor*. For a circular beam of radius a in a concentric chamber of radius b, it is g_f = 2 ln(b/a) + ½; for a rectangular chamber b should be multiplied by $4/\pi$. This expression contains both the contribution of space charge in the term ln a and that of the wall in the term ln b.

The voltage induced by the bunch current creates a local *potential-well distortion*, which slides up and down the applied rf voltage when the synchronous phase angle

changes with bunch current. The (coherent) synchrotron frequency of the bunch, which depends on the derivative of the rf voltage, therefore remains constant as long as the applied voltage is sufficiently linear. However, the (incoherent) synchrotron frequency of individual particles, given by the local derivative inside the potential well, not only depends on beam current but also varies between the center and the edge of a bunch. When the (square of the) synchrotron frequency in the center of a bunch is shifted below zero, an instability may occur, hence excessive potential well deformations should be avoided.

The mainly *inductive wall impedance* reduces the tune shift of the "*capacitive*" space charge, but is insufficient to compensate it in particular at injection energy. Thus it is useful to add more inductance, which can be done e.g. with *inductive inserts*, containing ferrite (Finemet) cores (see Chapter 5). Even at higher energies the space charge tune shift may be large if the bunch length is sufficiently small, e.g. due to reduced transition energy or rotation in phase space (see below). Again inductive inserts can be helpful. However, one has to take care that the total resistive part of the impedance is not increased excessively by them, as this determines the growth-rate of instabilities (see next section).

4.1.4 Effects of space charge on bunch rotation

In Phase I Stage 2 and Phase II, it is desirable to have short proton bunches (1–2 ns) impinging on the target for efficient production of muons and hence neutrinos. Therefore it was proposed to rotate the bunches in phase space just prior to ejection, converting their small energy spread into a short bunch length.

The minimum bunch length thus achievable is restricted by distortions of the bunch during phase space rotation. The speed of rotation of individual particles is given by their synchrotron tunes:

$$\nu_s = \sqrt{\frac{-\eta h V_{\mathrm{rf}} \cos\phi_s}{2\pi E/e}}\ , \qquad (4.7)$$

where V_{rf} is the applied rf voltage at frequency f_{rf} with harmonic number $h = f_{\mathrm{rf}}/f_0$, $f_0 = \omega_0/(2\pi)$ the revolution frequency, and the synchronous phase is ϕ_s. The *slip factor* $\eta = \gamma_T^{-2} - \gamma^{-2}$ expresses the distance to transition energy, and is negative below transition (for which cos ϕ_s is therefore chosen positive). η is only a weak function of energy when γ is not too close to γ_T, and then the variation of synchrotron frequency becomes only important for beams with large momentum spreads.

In the Proton Driver, the full momentum spread is usually quite small (7×10^{-4}). However, it has been proposed to reduce transition energy prior to ejection to shorten the bunches and require only little rotation in phase space. Strong distortions may result during bunch rotation due to the increased synchrotron frequency spread [7].

Longitudinal effects

For an intense proton bunch, the longitudinal space charge force will counteract the focusing rf force, thus reducing the synchrotron tune and slowing down the rotation rate. This cancellation becomes larger and larger as the bunch becomes shorter and shorter during the rotation. Sometimes, this space charge force will even be larger than the rf focusing force, making the particles rotate in the reverse direction in longitudinal phase space. Theoretically this is an instability of the synchrotron motion, which, however, is unimportant here, because we are interested in only about $\frac{1}{4}$ of a synchrotron period. The space charge modification of the rf potential occurs only near the core of the bunch where the particle intensity and therefore space charge is most intense. Ironically, this longitudinal space charge force is actually beneficial to the bunch rotation. This is because the slowing down of the rotation near the core provides time for the particles near the separatrices to catch up. As a result, the fraction of particles in the tails of the rotated compressed bunch will be much less. Of course, when the space charge is too large, bunch lengthening dominates and bunch compression becomes impossible.

We believe that the effect of space charge distortion of the rf waveform is governed by the ratio of the space charge force to the rf force. Simulations show that bunch compression through rotation in the longitudinal phase space is feasible provided that [9]

$$\frac{\text{Sp-ch force}}{\text{Rf force}} = \frac{eN_b|Z/n|_{sc}}{\sqrt{2\pi}h\omega_0^2\sigma_\tau^3 V_{\text{rf}}} \lesssim 17\ , \qquad (4.8)$$

where N_b is the number of particles in the bunch $(Z/n)_{\text{sc}}$ is the longitudinal space charge impedance per harmonic, and σ_τ is the desired rms bunch length after compression. From Table 4.3, it is evident that for Phase I Stage 2 of the Fermilab proton driver, the space-charge-to-rf ratio is very much less than the critical value of 17 stated in Eq. (4.8), implying that the longitudinal space charge constitute negligible influence on the bunch compression.

For Phase II operation, a compression to σ_τ = 1 ns is still possible, because of the σ_τ^3 dependency in Eq. (4.8) and the space-charge-to-rf ratio is only slightly larger the critical value.

A shortcoming of the bunch rotation method is the possible development of microwave instability when the rf voltage is reduced adiabatically to a small value so that the bunch will fill the whole bucket prior to the rotation. This can be avoided if the synchronous-phase-shift method of compression is used instead. The synchronous phase is first shifted from the center of the bucket to an unstable fixed point. The bunch is allowed to spread out along one set of separatrices. Later the synchronous phase is shifted back to the center of the bucket. The bunch is allowed to rotate in the longitudinal phase space for about $\frac{3}{8}$ of a synchrotron period and the shortest bunch results. This method gives a theoretical linear compression ratio of $\sqrt{2}/(\sqrt{3}\sigma_\phi)$, where σ_ϕ is the initial rms

bunch length measured in rf phase. Of course, final rotation will introduce nonlinearity and tails for the compressed bunch. However, this can be alleviated by extracting the bunch immediately at the end of the drift along the separatrices. The bunch is then sheared back to an upright position in the beam line via an optical system with local momentum compaction, or the R_{56} element of the transfer matrix.

Table 4.3. Comparison of the space-charge-to-rf ratio in bunch compression through rotation for Phase I Stage 2 and Phase II of the Fermilab proton driver

	Fermilab Proton Driver	
	Phase I	Phase II
Extraction kinetic energy (GeV)	16	16
h	18	18
Number per bunch N_b	$1.7\ 10^{12}$	$2.5\ 10^{13}$
Revolution frequency (MHz)	0.40932	0.40932
$\lvert Z/n\rvert_{sc}$ (Ohms)	2.639	2.639
$V_{\rm rf}$ (kV)	1400	1400
Extraction σ_τ (ns)	3	1
Sp-ch-to-rf ratio	0.060	23.9

Transverse effects

At the end of the bunch rotation in longitudinal phase space, the bunch will be compressed to its minimum length of, for example, $\sigma_\tau = 1$ ns with half momentum spread $\delta = \pm 0.0482$, where a bunch area of 2 eV-s has been assumed. (Actually, the momentum aperture of the proton driver is less than ±0.025. Thus to compress a bunch to 1 ns, the bunch area must be tailored to less than 1 eV-s to start with.) Although the extraction energy is high, the self-field space charge tune shift $\Delta\nu_{\rm sc}$ given by the first term of Eq. (4.1) can still be appreciable. It is possible that the reduction in betatron tune can modify the effective transition γ_T to such an extent that particles find themselves near transition. Higher order momentum compaction will be needed because of the large momentum spread. This may result in ruining the whole bunch rotation procedure as a result of nonlinearity.

Notice that the self-field space charge tune shift in Eq. (4.1) is inversely proportional to $\gamma^3\beta^2$. Thus, the tune shift is momentum dependent and can be written as

$$\Delta\nu_z \approx \Delta\nu_{sc}\left(1 - 3\delta + 12\delta^2\right), \qquad (4.9)$$

where $\Delta\nu_{sc}$ is evaluated at the nominal momentum. It is evident that the last two terms represent the first two lowest orders of chromaticity generated by the transverse space-charge force. In a Hamiltonian formalism, $\nu_z = \partial H/\partial J_z$, where J_z ($z = x$ or y) is the

transverse betatron action, which is related to the transverse offset z from the off-momentum closed orbit by $z = (2\beta_z J_z)^{1/2}$, and the *unnormalized* emittance ε by $\varepsilon = 2J_z$. For the simple case of a Kapchinakij–Vladimirskij (KV) beam [10] where the transverse distribution is uniform, $\Delta\nu_{sc}$ is J_z independent. Thus, the contribution of the self-field space charge tune shift to the Hamiltonian is [9]

$$\Delta H = \Delta\nu_{sc}\,(J_x + J_y)\left(1 - 3\delta + 12\delta^2\right) - \frac{\alpha_0 R}{2}\delta^2 \ , \tag{4.10}$$

where we have added the term contributing the nominal momentum compaction factor α_0. This Hamiltonian will result in a path length difference $\Delta\ell$ given by

$$-\frac{\Delta\ell}{2\pi} = \left\langle \frac{\partial \Delta H}{\partial \delta} \right\rangle = \Delta\nu_{sc}\,(J_x + J_y)\,(-3 + 6\delta) - \alpha_0 R\delta \ . \tag{4.11}$$

Here we arrive at an up-shift in the momentum compaction ($\Delta\nu_{sc}$ is negative)

$$\Delta\alpha_0 = -6\Delta\nu_{sc}\frac{J_x + J_y}{R} \ , \tag{4.12}$$

or down-shift of the transition gamma

$$\Delta\gamma_T = 3\Delta\nu_{sc}\gamma_T^3\,\frac{J_x + J_y}{R} \ , \tag{4.13}$$

which is dependent on the betatron oscillation amplitudes.

In Phase II of the Proton Driver, the number per bunch is $N_b = 2.5 \times 10^{13}$ and the rf harmonic $h = 18$. For the $\sigma_\tau = 1$ ns compressed bunch, the bucket bunching factor is $B_f \approx (2\pi)^{1/2} h f_0 \sigma_\tau = 0.01899$. With normalized 95% emittance $\varepsilon_N = 60\times10^{-6}\pi$ m, the self-field space charge tune shift is $\Delta\nu_{sc} = -0.297$. The maximum actions for betatron motion are only $J_x = J_y = 1.66 \times 10^{-6}$ m. However, most of the transverse beam size comes from the off-momentum dispersion. With a maximum dispersion[1] of $D \sim 3$ m, there is a contribution to the equivalent action at 2% momentum offset of $J_x = (D\delta)^2/(2\beta_x) \sim 0.00018$ m, where the horizontal betatron function has been taken as $\beta_x \sim 10$ m. With the nominal transition gamma of $\gamma_T = 27.71j$, the shift is only $\Delta\gamma_T = -0.031j$, which is small, and the particles are nowhere near transition.

It is important to point out that even if the transverse space charge force is very large, the modification to γ_T can be very much reduced by correcting the two lowest orders of

[1]A more accurate derivation should take into account the modification of horizontal dispersion and the introduction of vertical dispersion by the self-field space charge tune shift. See Ref. [11] for detail.

chromaticities. Although the self-field space charge tune shift actually contributes a spread in a non-KV beam, most particles, which reside in the core, will see roughly the same linear tune depression $\Delta\nu_{sc}$ and therefore a correction of the chromaticities will remedy the situation.

4.1.5 Computer simulation of beams with space charge

A number of computer codes exist which allow simulation of space charge effects in high current machines by tracking several thousands of super-particles over many turns. They are subjected to the effect of external focusing as well as to space charge forces. Some codes also permit inclusion of image effects.

At Fermilab, the longitudinal code ESME has been developed over more than 20 years for this purpose [8]. It has been used to optimize parameters by following particles from injection, through acceleration by rf cavities to their final energy. In particular, the evolution of energy and bunch length can be studied and the effect of inductive inserts optimized to minimize the loss of particles during injection.

The code TRACK-2D, developed in the Rutherford Laboratory in England [12], also includes transverse space charge effects, making use of a nonlinear space charge solver based on finite elements. Image charges, corresponding to an elliptical vacuum chamber, are also taken into account. The code has been applied to the parameters of the Fermilab Proton Driver to study the evolution of particles in transverse phase space. The results are shown in Figure 4.2 for the transverse plane (x, y), in Figure 4.3 for the horizontal phase space (x, x'), and in Figure 4.4 for the vertical phase space (y, y'). Each figure shows a sequence of shots in successive revolutions. These pictures give final transverse normalized 95% emittances of $\varepsilon_x = 69.5\times10^{-6}\,\pi$ m ($12.2 \times 10^{-6}\,\pi$ m rms) and $\varepsilon_y = 82.6\times10^{-6}\,\pi$ m ($12.4 \times 10^{-6}\,\pi$ m rms). The code has also been used to minimize the loss of particles at injection and keep the stripping foil from overheating by an excessive number of traversals. The foil is depicted as a rectangle in Fig. 4.2. The average number of foil hits per particle during the 27-turn injection cycle has been 1.4, in addition to the first passage when the electrons are stripped from the H^- beam. The code contains an improved calculation of space charge forces, and its longitudinal results have been in good agreement with previous ones obtained with ESME.

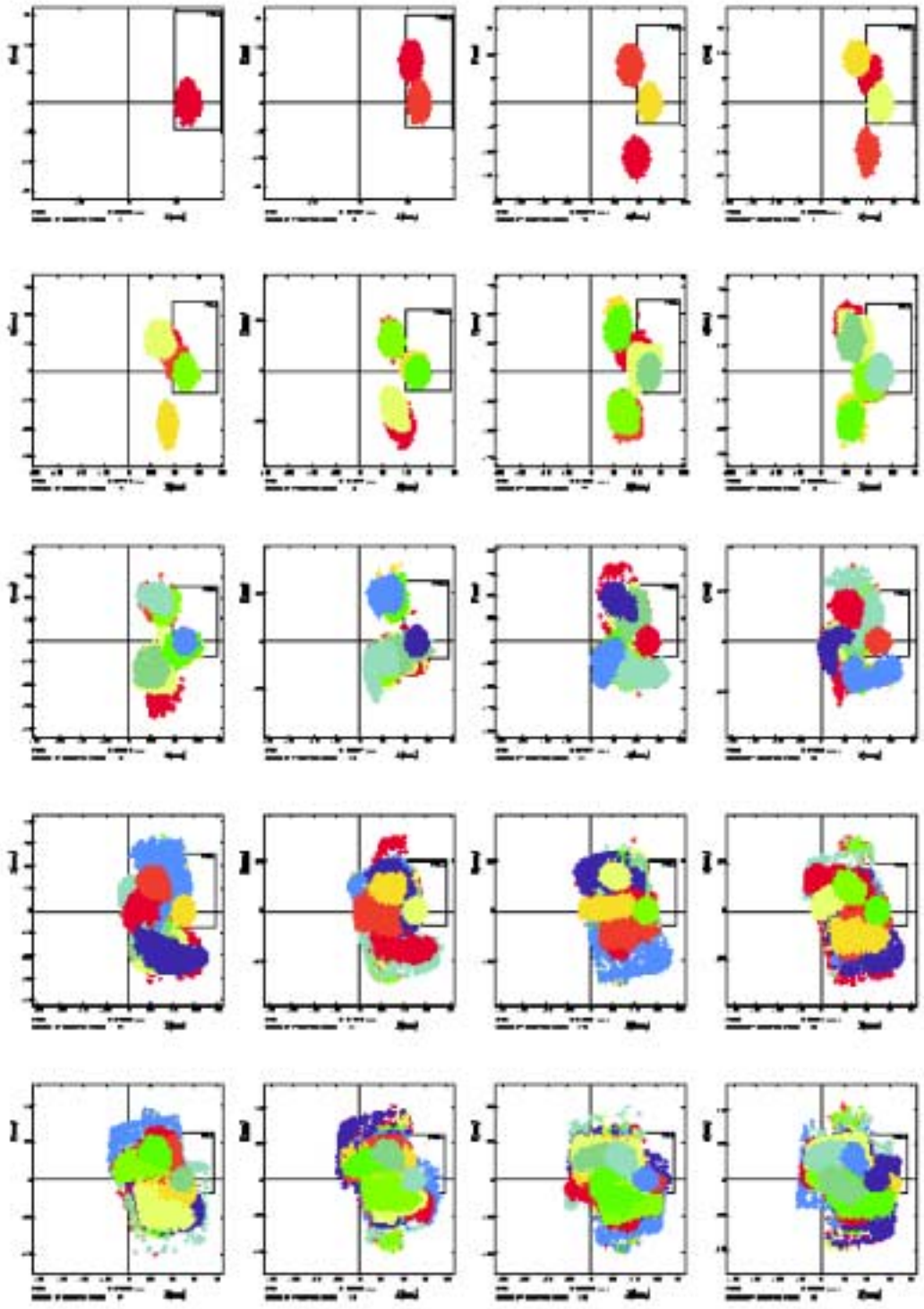

Figure 4.2. Plots of *x-y* at injection for the first 20 successive turns with space charge taken into consideration. The foil is depicted as a rectangle in each plot

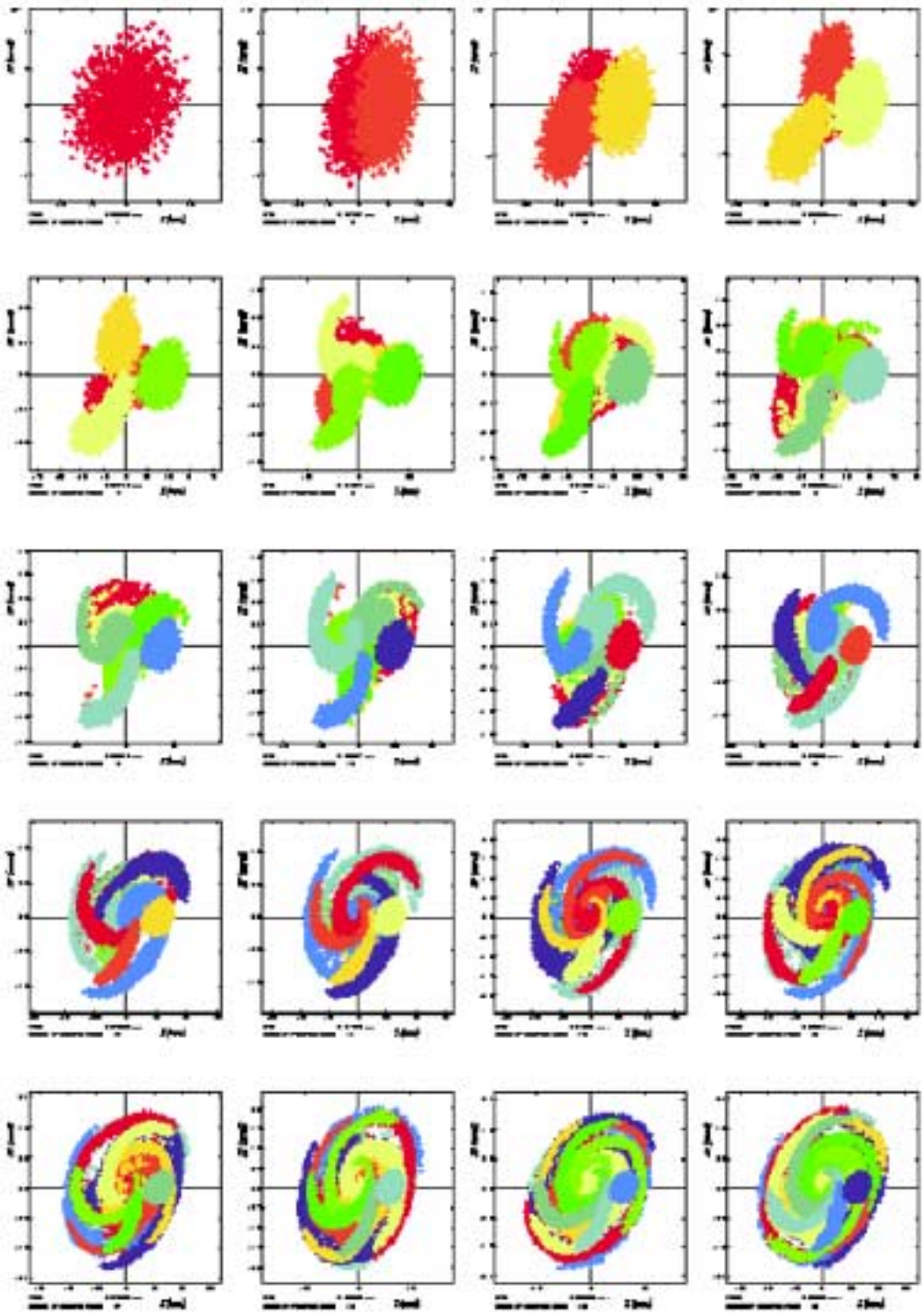

Figure 4.3. Horizontal phase space plots (*x*-*x'*) at injection for the first 20 successive turns with space charge taken into consideration

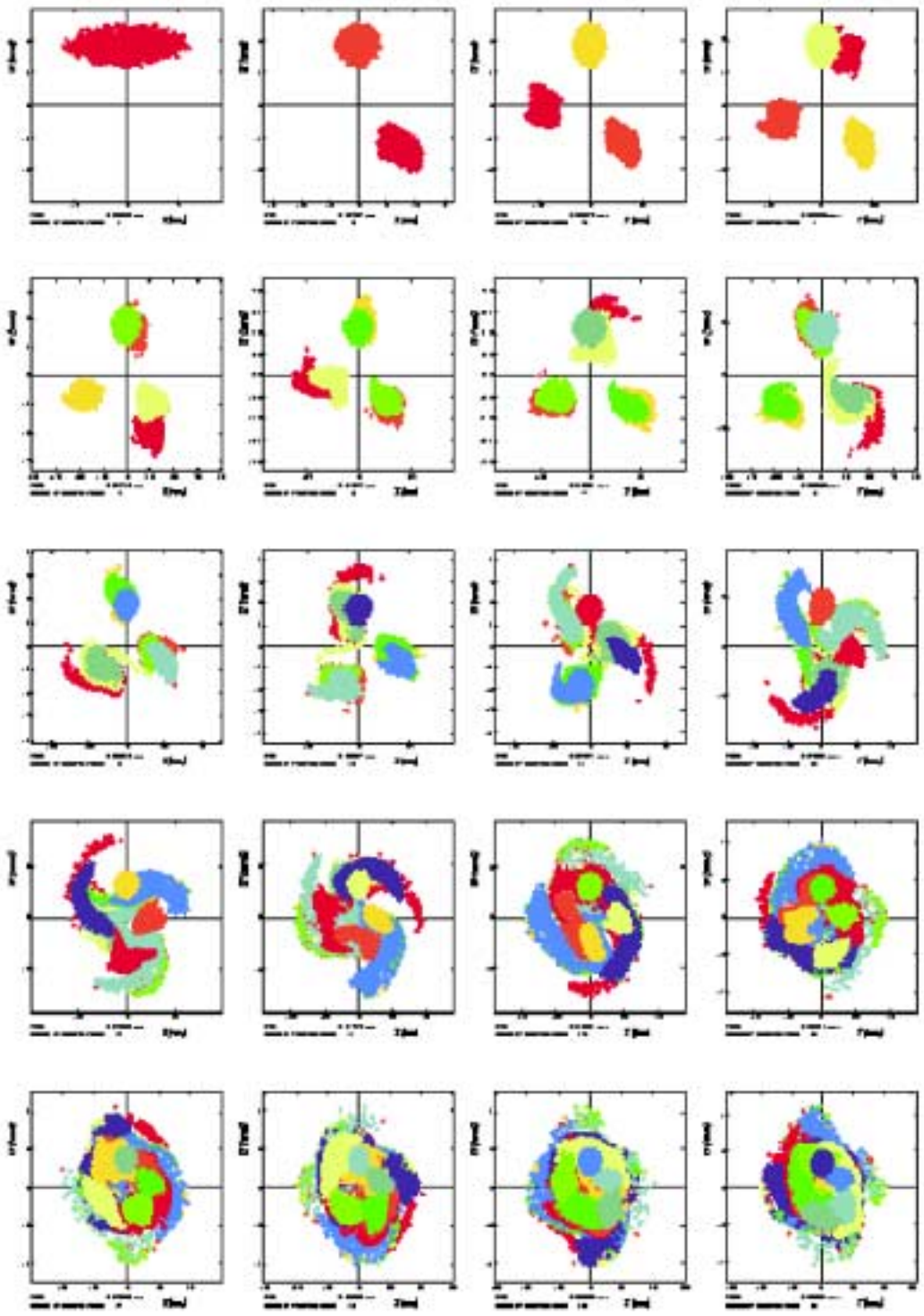

Figure 4.4. Vertical phase space plots (*y-y'*) at injection for the first 20 successive turns with space charge taken into consideration

4.2 Coherent Single Bunch Instabilities

4.2.1 Broad-band impedance estimates

The largest impedances in the Proton Driver, in particular at low energies, are due to space charge. They can be obtained from the last section [19]

$$\frac{Z_\parallel}{n}^{sc} = -j\frac{Z_0}{2\beta\gamma^2}\, g_f \ , \quad Z_{\perp_z}^{sc} = -j\frac{2RZ_0}{\beta^2\gamma^2}\left[\frac{1}{a_z(a_x+a_y)} - \frac{\xi_{1z}-\epsilon_{1z}}{b^2}\right] \ . \qquad (4.14)$$

The *g-factor* g_f was already given after Eq. (4.6). For a rectangular chamber with 5 to 9 ratio, the Laslett coefficients yield $\xi_1 - \varepsilon_1 = 0.412/0.223$ vertically/horizontally, and for an elliptic one 0.430/0.269. For a beam of radius a = 25 mm, in a chamber of radius b = 63 mm, the longitudinal impedance at injection energy is then about –371j Ω, while the transverse impedance reaches nearly –61j MΩ/m.

The finite conductivity of the vacuum chamber wall creates the *resistive wall impedance*, which contributes the largest real part to the impedance. It increases when the wall is made of high-resistance material such as Inconel or Ti alloys in order to reduce eddy currents.

For a material with conductivity σ_c, permeability $\mu = \mu_r\mu_0$, the *skin depth* at frequency ω is $\delta = \sqrt{2/(\omega\mu\sigma_c)}$. For a wall thickness larger than the skin depth, the longitudinal resistive wall impedance, divided by mode number $n = \omega/\omega_0$, of a circular cylindrical wall at radius b becomes

$$\frac{Z_\parallel}{n}^{rw} = (1+j)\beta\mu_r Z_0\frac{\delta_b}{2b} \ , \qquad (4.15)$$

assuming that the wall is thick compared to the skin depth. The transverse impedance is found simply by multiplication with $2R/(\beta b^2)$. The skin depths for various materials, evaluated at 300 kHz, the revolution frequency f_0 at injection energy, are shown in Table 4.4. The lowest betatron frequencies are smaller; f_0 is multiplied by the non-integer part of the tune q or $(1-q)$ if $q > \frac{1}{2}$. For simplicity, we give the skin depths and all impedances for the revolution frequency at injection energy. The transverse impedances have to be increased by the factor $q^{-1/2}$ or $(1-q)^{-1/2}$ once the exact tune is known.

Table 4.4. Resistive wall and space charge impedances at injection energy

Resistiv wall	ρ_c	σ_c	μ_r	δ	$Z_\parallel/n$	$Z_{\perp x}$	$Z_{\perp y}$
Material	$[\mu\Omega cm]$	[MS/m]		[mm]	[Ω]	[KΩ/m]	[KΩ/m]
Silver	1.59	62.9	1.0	0.12	0.247	5.53	19.7
Copper OF	1.71	58.5	1.0	0.14	0.256	5.74	20.5
Aluminum	2.91	34.4	1.0	0.30	0.337	7.49	27.1
SS Steel	57	1.75	1.001	0.4	1.48	33,2	118.4
Si-Steel 1%	23	4.34	9000	0.01	89.1	1998	7131.
Inconel	129	.775	1.002	0.92	2.22	49.9	178.0
Ti alloy	148	.676	1.0	1.07	2.38	53.4	190.5
Space charge					$-j371$	$-j60500$	$-j57200$

If the walls were made of good conductors, such as copper or aluminum, eddy current losses would be excessively high unless the metal was divided into narrow strips or wires, similar to the wire-cage used in ISIS [14]. The eddy current power loss per unit length in a metal strip of width *w*, height *h* and conductivity σ_c, at right angles to a changing magnetic field with time derivative *dB/dt*, is approximately given by $P/L = \sigma_c h w^3 (dB/dt)^2/12$. Since this is proportional to the third power of the width, it can be reduced from over 8 kW/m for a 1.3 mm thick, 22 cm wide, elliptic Inconel chamber to a few W/m by replacing it with 2 × 50 copper strips of 4 mm width and 50-100 μm thickness. For a metal thickness *t* small compared to the skin depth δ, the impedance given by Eq. (4.15) has to be multiplied by a factor $\delta/t > 1$. For the present case, this yields an impedance increase by about 3 for strips of 50 μm thickness, still tolerable due to the higher conductivity of copper.

For vacuum chambers made of ceramics, thin metal stripes of high conductivity can be deposited on the inside to shield the high impedance of the magnetic pole pieces behind them. However, such chambers need a thickness of 5-6 mm to withstand the pressure of air and thus would require larger magnet gaps for the full aperture. *Composite chambers* can be made slightly thinner, with a thickness of 2-3 mm, and would thus be preferable if their vacuum properties are found adequate.

Other sources of broad-band impedance are the rf cavities loaded with ferrite (or Finemet). Kicker tanks may create both broad-band and narrow-band impedances. Finally, bellows and other small cross-section variations of the vacuum chamber become important when they are present in large numbers, but have essentially mainly inductive impedance at low frequencies.

4.2.2 Shielding of electromagnetic fields by liners and cages

Although the skin depth is smaller for larger permeability, the additional factor μ_r in Eq. (4.15) makes the impedance large for magnetic material such as used for iron pole pieces. In particular if the pole pieces form part of the vacuum chamber as in the Fermilab Booster, they should be shielded in the Proton Driver where higher beam currents are desired. For this purpose, a screen or liner has been proposed, similar to the one being built as radiation shield for the LHC [13]. But to minimize eddy current losses, the screen for the driver should be made as thin as possible.

Therefore it is important to estimate the minimum thickness required to effectively shield the beam from the outer region. Assuming rotational symmetry, a screen of thickness *t* at radius *b*, with skin depth $\delta_b >> t$, and an outer wall at radius *d*, with skin depth δ_d, the *shielding condition* in the longitudinal direction can be written [18]

$$\frac{t}{\delta_b} \gg \frac{\beta^2\gamma^2}{2\ln(d/b)}\frac{\delta_b}{b} \approx \frac{\beta^2\gamma^2}{2}\frac{\delta_b}{d-b} \qquad (4.16)$$

where the second relation holds when $d - b << b$. At low energies, when $\beta\gamma$ is small, the required screen thickness *t* can thus be smaller than the skin depth by the factor δ_b / b, or $\delta_b /(d-b)$ when the screen is close to the outer wall.

A similar condition has been given for a metallized ceramic wall [17], where $(d - b)$ is replaced by the thickness of the ceramic wall. In the *transverse direction*, the shielding condition under the same assumption becomes simply [18] $t/\delta_b >> \beta^2\gamma^2\delta_b / b$, similar to the longitudinal criterion but without the logarithmic term. Hence for γ not too large, shielding in the transverse direction is always achieved when longitudinal shielding is good.

For higher energies, taking into account the finite skin depth at the outer wall, the criterion becomes $t/\delta_b >> (d/b)(\delta_b / \delta_d)$, i.e., the skin depth of the screen should be less than that of the outer wall. This is difficult to fulfill when the outer wall is ferromagnetic and thus has a very small skin depth. However, at higher energies the beam is more stable and the space charge part of the impedance is strongly reduced.

4.2.3 Longitudinal stability criteria

The simplified *Keil-Schnell* or *circle criterion* is often used to estimate longitudinal stability limits, but is really not applicable for space charge dominated beams, since the actual stability limit is very large for a capacitive reactance. For bunched beams, one has to replace average current I_b by peak current by dividing it with the bunching factor B_f. One thus obtains the *Boussard criterion* for the *microwave instability*

$$\frac{|Z_\parallel|}{n} < F\frac{|\eta|B_f E_0}{e\beta^2 I_b}\left[\frac{\Delta E}{E}\right]_{FWHM} . \qquad (4.17)$$

The *form factor F*—originally assumed to be of the order of unity—is much larger for a space charge dominated impedance. In Phase I, the total beam current with 3×10^{13} protons is 1.4 A in 126 bunches and I_b only 12 mA. The bunching factor is about 0.5 near injection energy $E = \gamma E_0 = 1.3$ GeV, E_0 being the rest energy. The full energy spread is then 7×10^{-4}, and the full spread at half height about $\sqrt{2}$ smaller. Even with $F = 1$ one finds a quite comfortable limit of over 12 kΩ at injection when the particle energy is at its lowest value. The transition gamma of $\gamma_T = 27.71j$ has been used although the result is not sensitive to it at injection. For Phase I Stage 2, the same current is divided into only 18 bunches; the threshold with the same form factor of unity is still several kΩ and hence no problem is expected from microwave instability.

4.2.4 Transverse stability criteria

The situation is more critical in the transverse case. The lowest oscillation frequency is smaller than the revolution frequency, multiplied by the non-integer part of the tune $q = \nu_z - \mathrm{int}(\nu_z)$, or its complement $(1 - q)$, whichever is smaller. This impedance is quite large at very low frequencies, but mainly on one or two narrow spectral lines. The effective broad-band impedance is obtained by integrating over the bunch spectrum. For a centered spectrum, the resistive part is thus quite small as $Z_\perp(\omega)$ has opposite signs for positive and negative frequencies. However, when the transverse bunch spectrum is shifted by chromaticity ξ_z, the real part of the effective broad-band impedance due to finite wall resistivity can become quite large.

The growth rate of the *head-tail instability* for a beam consisting of n_b equally spaced bunches, each with average bunch current I_b, can be written as [16]

$$\frac{1}{\tau} = -\frac{1}{m+1}\frac{en_b I_b c}{4\pi\nu_z E}\sum_k \mathcal{R}e\, Z_\perp(\omega_k)F'_m(\omega_k - \chi_z) , \qquad (4.18)$$

where $\chi_z = -\xi_z\omega_0\tau_L/\eta$ is the *chromatic phase shift* across the full length τ_L of the bunch. The spectrum of frequencies for the m^{th} mode of transverse oscillations with *coupled bunch mode number n* $(0 \le n < n_b)$ is given by

$$\omega_k = kn_b + n + \nu_z + m\nu_s . \qquad (4.19)$$

The form factor $F'_m(\omega)$ expresses the cancellation occurring in the summation over both positive and negative frequencies of the real parts of the impedance, weighted by the spectrum of the m^{th} mode of oscillation. In practice, mainly mode $m = 0$ is of concern, which can be damped below transition by *negative chromaticity*. The higher modes, $m \ge 1$, are damped by a tune spread of order $1/(\omega_0\tau_L)$ which usually occurs naturally.

Ferrite loaded cavities and inductive inserts may contribute a large broad-band impedance, with a resistive part, which becomes large at frequencies where the ferrites become lossy. Fortunately, most ferrites have low losses below 100 MHz where the resistive wall contribution is highest.

4.2.5 Cures

Inductive inserts can be effective for compensating the "capacitive" space charge impedance. However, they require considerable space around the machine. Ferrite with small losses at lower frequencies should be chosen to limit the resistive impedance.

It is further prudent to keep transition well above the highest operation energy by designing a lattice with small or imaginary momentum compaction. A reduction of transition to limit the required bunch rotation could be dangerous and should be applied only very shortly before the beam is ejected.

4.3 Coupled Bunch Instabilities

4.3.1 Narrow-band impedance estimates

We already mentioned the resistive wall impedance, which is in particular high in the transverse plane at the lowest betatron frequency $q f_0$, which is about 100 kHz for $q = 0.33$. For a thick Inconel wall at $b = 63$ mm, with a skin depth of 1 mm, $Z_\perp \approx 200$ kΩ/m, but for a very thin one, such as proposed for shielding the pole pieces, the value would be much higher, e.g. 40 times for a thickness of 25 μm.(1 mil). For copper, with a nearly hundred times better conductivity, all values are 10 times lower.

In addition, we have to include narrow band resonances of higher order modes (HOMs) in rf and other cavities, such as kicker tanks for injection or ejection. For Stage 2 of Phase I, the 5 MHz rf cavities will be either tuned or damped by ferrite (or Finemet) and their losses will damp most HOMs. However, for Stage 1, with a 53 MHz rf system, the cavity modes must be measured and either damped internally or coupled out to a load. Measurements should be made when a prototype of these cavities becomes available.

Also the kicker tanks should be designed to permit damping of the HOMs by similar means. Sometimes it is already sufficient to use lossy material for the insulators inside these tanks.

4.3.2 Longitudinal stability criterion

Coupled-bunch modes will become unstable in a beam of n_b equally space bunches with equal average currents I_b when the imaginary part of the complex frequency shift $\mathrm{Im}(\Delta\omega_{mk})$ exceeds the frequency spread [15]. Here $m \geq 1$ is the *azimuthal mode number*

(m = 1 dipole, m = 2 quadrupole, etc.), and $0 \le k < n_b$ the *modal mode number* of an oscillation with phase shift $\Delta\phi = 2\pi k / n_b$ between adjacent bunches [15]:

$$\Delta\omega_m = \frac{2m}{m+1}\frac{E_0 I_b}{e h V_{\rm rf} cos\phi_s}\left(\frac{Z_\parallel}{n}\right)_{\rm eff}^{(m,k)} , \qquad (4.20)$$

where the *effective impedance* is defined as the (infinite) sum over the product of the impedance $Z_\parallel / n$ and the power density $h_m(\omega)$, evaluated at all spectral frequencies $\omega_{mkp} = \omega_0(pn_b + k + m\nu_s)$, and normalized by the sum over all power densities:

$$\left(\frac{Z_\parallel}{n}\right)_{\rm eff}^{(m,k)} = \sum_{p=-\infty}^{\infty} \frac{Z_\parallel}{n}(\omega_{mkp}) h_m(\omega_{mkp}) , \qquad (4.21)$$

where the power spectrum $h_m(\omega)$ of the m$^{\rm th}$ mode of oscillation has been normalized such that $\sum_p h_m(\omega_{mkp}) = 1$.

For a single resonance at frequency ω_r, with shunt impedance R_s and quality factor Q, the growth rate of the *longitudinal coupled bunch oscillations* can be written as

$$\frac{1}{\tau} = -\frac{|\eta| n_b I_b R_s f_0}{2\pi\nu_s B_f} \mathcal{R}e[D(\alpha_d) F_m(\Delta\Phi)] , \qquad (4.22)$$

where $\alpha_d = \omega_r \tau_{sep} /(2Q)$ is the decrement between bunches separated by τ_{sep}. The function $D(\alpha_d)$ is unity for small arguments, and decreases rapidly for larger ones. The form factor F_m is a function of the phase shift across the bunch $\Delta\Phi = \omega_r \tau_L$. It has maxima for the $m^{\rm th}$ mode when the argument is $m\pi$, decreasing approximately as 1/m.

The required damping of the higher modes in the rf cavities, kicker tanks and other incidental cavities can be calculated only when their frequencies, shunt impedances and quality factors have been measured. Computer programs like BBI [20] or ZAP [21] can be used to perform the necessary summations over all impedances.

4.3.3 Transverse stability criterion

The criterion for stability against transverse coupled bunch modes can be written as [16]

$$|Z_{\perp z}| < F\frac{4B_f E}{e\beta\langle\beta_z\rangle I_b}\left[\frac{\Delta E}{E}\right]_{\rm FWHM} |S_z| , \qquad (4.23)$$

where the *effective tune spread* is $S_z = (n - \nu_z)\eta + \xi_z$, with n an arbitrary integer. However, instability occurs only for *slow waves* with $n > \nu_z$. The form factor F depends on the transverse particle distribution, but is large compared to unity for a space charge dominated impedance as in the longitudinal case.

Stability becomes particularly critical when the spread $|S_z|$ is very small, which can happen when its two terms nearly cancel. For the proton driver, operating below transition energy, the slip factor $\eta = \gamma_T^{-2} - \gamma^{-2}$ is negative. If the chromaticity ξ_z also is negative, the two terms add and cannot cancel. The lowest value of the spread is obtained for n just above the tune ν_z. Since also $|\eta| \approx ½$, the first term in S_z can be neglected if the (negative) chromaticity is large enough. For $F = S_z = 1$, the transverse impedance threshold is approximately 14 MΩ/m. Hence the transverse impedance of over 50 MΩ/m could make the beam unstable. However, stability is already achieved with a form factor $F = 2$ and a chromaticity $\xi_z = -3$.

4.3.4 Cures

The design of the vacuum chamber and the choice of material for the chamber walls are most important to keep the resistive wall effect small. Sufficient shielding of the magnetic pole pieces is necessary if they form part of the vacuum chamber or are separated only by ceramic or composite walls.

The obvious cure for HOMs of the cavities is damping by lossy material inside or by coupling the offensive modes into a load. A larger energy spread would increase the safety margin for Landau damping and could be obtained simply by increasing the (negative) chromaticity. The transverse feedback system would only be required for the lowest unstable oscillation frequencies and could thus be rather inexpensive.

4.4 Electron-Proton Instability

4.4.1 Equations of motion

When a proton beam is partially neutralized, with fractional neutralization χ_e, the electrons in it will start to oscillate transversely with the so-called *bounce frequency*. For small amplitudes it is given by

$$\omega_e^2 = 4c^2 r_e n_p \,, \qquad (4.24)$$

where $r_e = 1.535 \times 10^{-15}$ m is the classical electron radius, and $n_p = N_p/(\pi a_x a_y L_b)$ is the volume density of the protons in a bunch with N_p protons, cross section $\pi a_x a_y$ and full length L_b.

The oscillating electrons will also excite the protons to oscillate with frequency

$$\omega_p^2 = 4c^2 r_p n_e = 4c^2 r_p \chi_e n_p \ . \qquad (4.25)$$

The coupled oscillations lead to a dispersion relation for the *e-p oscillation frequency* ω as a function of the azimuthal mode number *n*:

$$(\omega_e^2 - \omega^2)[\omega_\beta^2 + \omega_p^2 - (n\omega_0 - \omega)^2] = \omega_e^2 \omega_p^2 \ . \qquad (4.26)$$

The amplitudes of the lighter electrons will grow rapidly, while the oscillations of the heavier proton remain smaller. When electrons reach the vacuum chamber wall, more electrons may be generated by *secondary emission*, which can lead to an avalanche effect called *multipactoring*. This may then lead also to emittance growth or beam loss of the protons.

4.4.2 Observations

Electron-proton oscillations have been seen in a number of *proton storage rings* (PSRs), and were overcome by different means. In a small PSR at the INP in Novosibirsk, constructed mainly for the study of charge exchange injection, these oscillations could be overcome by a simple feedback system. In the CERN ISR, electrons impinging on the chamber wall caused periodic background spikes, and had to be eliminated by better clearing and pumping. However, at the PSR in Los Alamos (LANL), the e-p instability was limiting the beam current for many years to values below the design goal. All attempts to eliminate or at least reduce the number of electrons failed.

The most common method to reduce neutralization of a beam is to leave a gap in the train of bunches; this has also been foreseen for the Fermilab proton driver. A more active method is to install clearing electrodes, and eliminate the electrons by applying transverse electric fields. If the electrons are generated by vacuum, better pumping may help—but not if the electrons are coming from the H^- stripping foil. Multipactoring at the wall can be reduced by coating with a material with a low secondary emission coefficient, such as Ti-N. If nothing else helps, a feedback system can be the solution. For the case of the LANL PSR, all these methods were tried and failed, and only a combination of higher rf voltage, sextupoles, partial wall coating and finally an inductive insert permitted reaching the design current.

A particular encouraging experience comes from the spallation source ISIS, where no e-p instability has ever been seen, even when the vacuum pressure was increased by switching off several pumps. The instability did not even occur when the machine was not running as a rapid-cycling synchrotron but with stored beam. This observation is not fully understood, and further studies are being made, both theoretically and experimentally.

The main conclusion is that a very low vacuum is mainly required for storage rings, not for a rapid cycling synchrotron as the Proton Driver where the beam is present only

for a short time. Furthermore, electrons are created by many other processes in addition to residual gas ionization. A vacuum at level 10^{-7} Torr is therefore considered sufficient. This is still economically achievable even with the magnet inside the vacuum, which has a rather high out-gassing rate due to various exposed epoxy surfaces. This approach, shielding by a liner made from copper strips to reduce the impedance of the exposed ferromagnetic pole pieces while keeping eddy current losses small, is presently considered the preferred solution for the vacuum chamber of the Fermilab Proton Driver.

References

[1] J. Laslett, BNL Report 7534, (1963) p. 234.
[2] Z. Qian, private communication.
[3] S. Wolfram, MATHEMATICA, Cambridge Univ.Press (1996).
[4] R. Baartman, AIP Conf. Proc. 448 (1998) p. 56.
[5] A. Chao, M. Tigner, Handbook Accel. Physics, World Scientific (1999).
[6] A. Chao, Physics of Collective Beam Instabilities, Wiley (1993).
[7] J. Norem, et al, Proc. PAC Vancouver 1995, p. 396; D. Trbojevic, et al, Proc. PAC Vancouver, 1995, p. 1030.
[8] J. Maclachlan, et al, Fermilab Report 1650, 1990.
[9] K.Y. Ng, Fermilab Report FN-702, 2000.
[10] I.M. Kapchinakij and V.V. Vladimirskij, Proc. 2nd Int. Conf. on High Energy Accel. and Instr., CERN, Geneva, 1959, p. 274.
[11] S.Y. Lee and H. Okamoto, Phys. Rev. Lett. **23**, 5133 (1998).
[12] C. Prior, Track-2D, private communication.
[13] F. Caspers, Proc. PAC New York, 1999, p. 1408.
[14] I. Gardner et al, Part. Accel. **31**, 227 (1990).
[15] F. Sacherer, CERN Report CERN/MPS/BR 73--1, 1973; IEEE-NS **20**, 3, 825 (1973). Proc. PAC San Francisco, 1973.
[16] F. Sacherer, CERN Report 77-13, 1977.
[17] A. Piwinski, DESY Report 1978.
[18] R. Gluckstern, US Acceler. School, Phoenix, AZ, Jan. 2000, to be published as a CERN Yellow Report.
[19] D. Moehl, A. Sessler, "rf knockout," LBL Report 1970.
[20] A. Hofmann, et al, IEEE-NS **26**, 3514 (1979).
[21] M. Zisman, et al, LBL Report 21270, 1985.